Chapter 3

Characterisation of Thin Drug-Loaded Poly(l-lactic acid) Films

3.1 Introduction

Polymeric delivery systems have proven to be an effective means for the controlled delivery of drugs both in terms of the ability to programme the kinetics of release and the ability to target the location of delivery. One such polymeric delivery system that has received significant attention over the last decade is the drug eluting coronary stent, where the drug is dispersed within a thin biodegradable polymer film on the metal stent[1]. As the polymer degrades the drug is intended to be released in a controlled and predictable way to the local tissues. However, such thin polymer films provide considerable challenges both in terms of fabrication and of particular interest to this thesis, characterisation. One of the key factors that control the kinetics of release is the distribution of drug throughout the film and hence, fabrication procedures attempt to ensure uniform drug distribution. A range of techniques have been applied to elucidate drug distribution within polymer films with varying levels of success[2-5], described in Chapter 1. In this chapter the first use of XPS depth profiling to quantitatively characterise the drug distribution in thin biodegradable polymer films representative of drug eluting stent coatings is described illustrating its utility in this type of biomaterial system and compared with more established ToF-SIMS depth profiling. Surface XPS and ToF-SIMS have previously been shown to be complementary in the data generated[6, 7]. This chapter will examine the data produced by both through thickness.

XPS provides a quantitative understanding of the distribution of components within the blend whereas ToF-SIMS produces a more qualitative understanding of where components are distributed. Analysis of the data provided by both methods allows for a comparative analysis of the two techniques for depth profiling purposes. This is crucial in establishing the value of new techniques such as XPS depth profiling for biomaterial analysis.

As described in Chapter 2 modern sputtering sources allow us to depth profile organic material with little damage compared to traditional sputtering sources such as caesium and argon. The purpose of such sources is to generate meaningful information, in this case the local concentration of codeine within a blend. Detailed studies of single component polymer films have been undertaken previously which have shown the properties of a range of polymers when depth profiling[8-10]. Such studies have shown that PLA is highly suited to depth profiling indicating a uniform sputter rate up to 1 μm into the depth of it at room temperature although at low temperature it has been shown a greater depth can be achieved[11-13]. Owing to its suitability for the model and amenability to sputtering PLA is selected as the polymer of choice in this model.

Very recently, time of flight secondary ion mass spectrometry (ToF-SIMS) using coronene primary ions, a planar aromatic hydrocarbon $C_{24}H_{12}^{+}$ shown in Figure 3.1, has been shown to exhibit similar performance to the well established organic sputtering source C_{60}^{+}[14] and as such, may be applicable for the depth profiling of drugs in polymers.

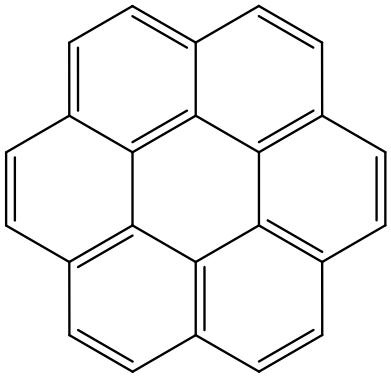

Figure 3.1 Molecular structure of coronene.

XPS depth profiling of thin organic films has been reported using a C_{60} sputter source showing that cluster ion sources are useful within the field of biomedical polymer analysis but it has not yet been employed to investigate drug loaded polymer systems[15-18]. Previously, the damage build up in organic films when etched using monatomic argon ions, found on all surface analysis instruments and intended for sputtering metal and inorganic samples, prevented such experiments

as the useful molecular ion intensities were found to degrade within seconds of sputtering[19, 20].

Codeine ($C_{18}H_{21}NO_3$) is selected for this work as its fragmentation under ToF-SIMS has been previously researched at Nottingham[21] and is generally understood making it suitable as a drug in this model system. It is an opioid analgesic similar to morphine but with less potent properties, it has a low molecular weight with a *m/z* of 299. The molecular ion $[M+H]^+$ is found at *m/z* 300 which is a unique ion which can be monitored for SIMS experimentation. Codeine is readily soluble in chloroform as is PLA, where the PLA (55 kDa) is otherwise insoluble in water but will instead hydrolyse slowly. By using PLA and codeine for a model of drug/ polymer blends the physiochemical properties of the constituents are known and the diagnostic secondary ions have been identified. With *a priori* knowledge allows for more efficient analysis of the hyperspectral data generated. The initial surface chemical analysis with ToF-SIMS utilised Ga^+ primary ions (data not shown), but subsequently bismuth clusters were preferably used as they are capable of producing greater intensity of larger ions such as that of codeine at *m/z* 300 as described in Chapter 2.

The aims of this chapter are to develop a drug/polymer model film suitable for depth profiling with XPS and ToF-SIMS to determine whether the data obtained through thickness are comparable and complementary. The techniques will be judged on the quality of the depth profiles they are able to yield throughout the model films. The determination of inferences regarding the expected release and performance of these model films through full characterisation of the constituent distribution is also an aim of this work.

3.2 Experimental

3.2.1 Sample Preparation

Silicon wafers measuring 1 cm^2 were treated with piranha solution (consisting of a 3:1 mixture of 98% H_2SO_4 and 30% H_2O_2 in water) for 30 min, followed by thorough rinsing with deionised water and drying with gaseous nitrogen before

being used as the substrate for spin casting. Solutions containing 20 mg of PLA (Polysciences, Warrington, PA) per ml of chloroform with 0%, 2.4%, 4.7%, 9.1%, 16.7% and 28.6% codeine (Sigma Aldrich) were produced thereby yielding a range of drug loadings. The solutions were spun cast at 4000 rpm for 60 s using a Cordell spin coater Mk. 7 (Cordell Group, Stockton-on-Tees). Five separate drug loadings (2.4%, 4.7%, 9.1%, 16.7% and 28.6% w/w codeine:PLA) were produced in addition to a pure PLA reference sample.

3.2.2 Ellipsometry

Ellipsometry was undertaken using an M – 2000DI spectroscopic ellipsometer (J. A. Woollam Co., Inc., Lincoln, NE). A triplicate of uncoated silicon wafers were used to ascertain the thickness of the SiO_2 layer. The highest and lowest drug loaded samples (produced from solutions containing pure PLA and 28.6% w/w codeine:PLA) was used to produce a model for ellipsometrically deriving drug loading within all films, assuming the films were transparent in this region (extinction coefficient, k=0) and the dispersion in refractive index (n) could be approximated with a two parameter Cauchy function shown in Equation 3.1.

$$n = A + \frac{B}{\lambda^2} \qquad \textbf{Equation 3.1}$$

The ellipsometric data was acquired at high wavelengths (>500 nm). The wavelength-dependent optical constants n and k were then calculated across the whole wavelength range (195 nm to 1700 nm) through a direct inversion of the ellipsometric data. The extracted values were then fitted with a Kramers-Kronig consistent dispersion function using Gaussian oscillators[22] to provide wavelength-dependent values of n(PLA), n(28.6% codeine) and k(PLA), k(28.6% codeine). This is done in order to model the absorption spectrum of the material analysed. This was undertaken using an effective medium approximation (EMA) model which models the absorption spectrum of the material being analysed with ellipsometry and is capable of reporting a percentage estimate of the proportion of the film containing one of the two components[23, 24].

In this analysis, it was assumed that the optical constants for films with an intermediate codeine drug loading are a linear combination of those of the pure PLA and the highest codeine film. This is a relatively safe assumption to make as PLA has no absorption in the wavelength region acquired whereas codeine does. Thus, n = a.n(PLA) + (1-a).n(28.6% codeine) at every wavelength; k is derived analogously. The value 'a' is a constant for each sample which represents the volume fraction of codeine normalised to the 28.6% codeine sample. All samples were fitted using 'a' and the thickness as variable parameters for the overlayer film, excellent fits were obtained in all cases.

3.2.3 Atomic Force Microscopy

AFM used a MultiMode Scanning Probe Microscope (Veeco, Santa Barbara, CA, USA). All measurements in this chapter were performed with tapping mode in air, using silicon nitride probes. At least three different areas were analysed on all samples presented and topography and phase images are recorded simultaneously. In this chapter all images are acquired of a 10 × 10 μm region. All AFM topographical analysis was performed on a Nanoscope version 6.13 (Veeco).

3.2.4 X-ray Photoelectron Spectroscopy

The XPS spectra were acquired using an Axis Ultra DLD spectrometer (Kratos Analytical, UK) with a monochromated Al K_α source producing a 450 W energy. The data was converted to VAMAS format and processed using CasaXPS, version 2.3.14. High resolution C1s, N1s, O1s and Si2p spectra were collected at a pass energy of 80 eV and a step size of 0.1 eV and quantified using empirically derived relative sensitivity factors provided by Kratos Analytical. The pressure in the analysis chamber was maintained below 2×10^{-8} mbar for data acquisition. The coronene primary ion source was mounted at 45° to the sample surface which itself was normal to the analyser. The coronene beam was operated at 12 keV energy and only $C_{24}H_{12}^{+}$ (singly charged polyatomic ions) were used for depth profiling. This selection was made using a Wein mass filter. The raster size was fixed at 2.5 × 2.5 mm. XPS spectra were collected using a 110 μm aperture. Due

to time constraints only the 2.4%, 9.1% and 28.6% (w/w) codeine loadings were analysed with XPS depth profiling.

3.2.5 Time-of-Flight Secondary Ion Mass Spectrometry

A ToF-SIMS IV time-of-flight secondary ion mass spectrometer (ION-TOF GmbH, Münster, Germany) was used for all ToF-SIMS work undertaken across the experimental chapters. Three ion sources have been used in my analysis, a $^{69}Ga^{+}$ liquid metal ion source using an acceleration voltage of 25 keV and an AC target current of 1.26 pA with a bunched pulse width of less than 0.2 ns. $^{209}Bi^{+}$ liquid metal ion source set to an acceleration voltage of 25 keV and a target current of 1 pA was used along with $^{209}Bi_3^{+/++}$ cluster ions, the target current of the bismuth varied depending on the charge of the cluster. Finally a $^{720}C_{60}^{+}$ source was also used for sputtering using an acceleration voltage of 10 keV and a target current of 200 pA was strictly adhered to. The target current was measured after each depth profile to ensure reproducibility of sputtering across samples analysed.

3.3 Results and Discussion

3.3.1 AFM

AFM was first employed to characterise the surface of the spin cast films in order to confirm whether the films produced were uniform, continuous and thus appropriate for comparative depth profiling. The initial casting of these films on either chloroform and hexane solvent cleaned silicon wafers or those after piranha solution cleaning are shown in Figure 3.2.

a. b

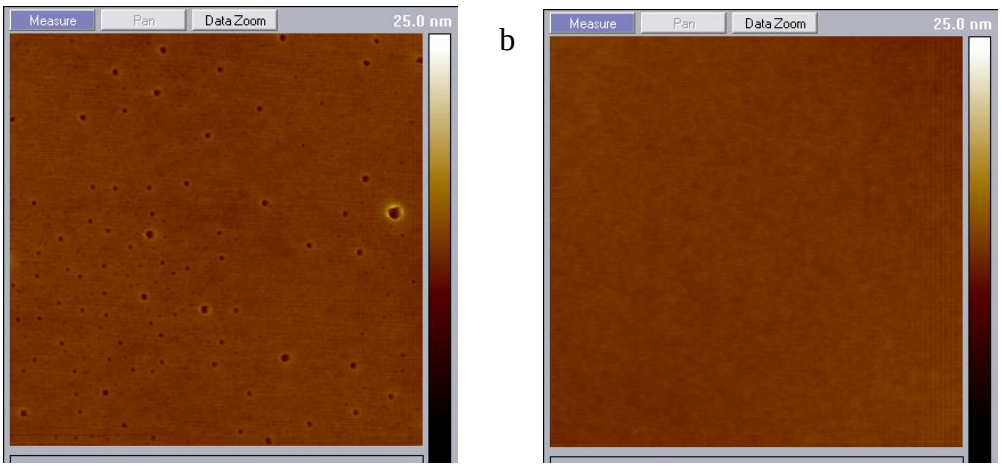

Figure 3.2 Representational AFM images for a 10 × 10 µm area of a (a) solvent cleaned and a (b) piranha solution cleaned silicon wafer with a 28.6% (w/w) codeine/PLA blend film deposited at 4,000 RPM for 60 s.

Holes in the polymer film are evident across all films analysed with the solvent cleaning method. In contrast, the film is continuous at the surface of the substrate that was piranha cleaned and therefore suitable for depth profiling. The presence of such holes has previously been explained as the evaporation of highly volatile solvent from within the casting solution after the termination of the spin casting process[25]. The results observed with piranha solution cleaning of these films indicate a dewetting phenomenon at the silicon wafer interface with the thin film. Similar phenomena of solvent related dewetting of the silicon dioxide layer has previously been described for thin polyethylene films[26].

A discontinuous film indicates there is likely to be variation in the rate at which C_{60} or coronene ions will sputter the surface with data being acquired from multiple heights simultaneously. This can skew the data from the resultant depth profiles, assuming variation between the surface and bulk of the thin films. All silicon wafers produced subsequently and for casting utilised piranha solution cleaning. AFM analysis did not show any phase separation of PLA and codeine in these blends across the concentration ranges studied and the phase images produced. As such the surface morphology and topography explored by AFM suggests a homogeneous distribution of the miscible PLA/codeine binary blend across the range of mixtures studied.

3.3.2 Ellipsometry

The consistency of drug loading and the thickness of doped PLA films were examined using spectroscopic ellipsometry for 3 replicates of each of the 6 drug loadings. The films were optically homogenous and isotropic, satisfying the criteria for modelling the spectra obtained using ellipsometry. Knowledge of the thickness of the films allows for rationalisation of the depth scale, allowing for a sputter rate to be determined assuming uniform sputtering. The SiO_2 layer on the uncoated silicon wafers measured 2 nm in thickness and it was this value which was subtracted from all results. It was noted that the film thickness was highly consistent when cast from solutions with identical drug loadings, exhibiting a maximum value for the coefficient of variation of 2.9% shown in Figure 3.3.

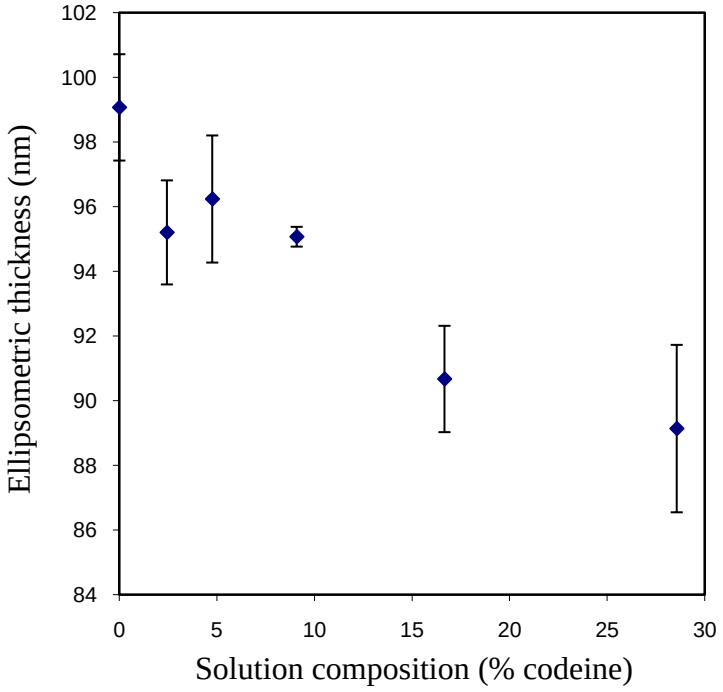

Figure 3.3 Film thickness of PLA and PLA/codeine blends determined using ellipsometry.

The film thickness ranges from 86.2 nm to 100.3 nm for the maximum codeine concentration to the pure PLA. Through its longer chain length and higher viscosity than codeine, PLA is most responsible for variation in film thickness. In the highest drug loadings more codeine was added to the PLA, as weight percentages were used a greater volume of chloroform was required to produce a

20 mg/ml solution, having a diluting effect on the PLA hence reducing film thickness with an increase in drug concentration.

There was a good correlation (R^2 = 0.9979) between the solution composition, or drug loading, and the relative composition of the films generated from spectroscopic ellipsometry shown in Figure 3.4. This confirms that the fraction of codeine in the films scales linearly with the fraction in solution.

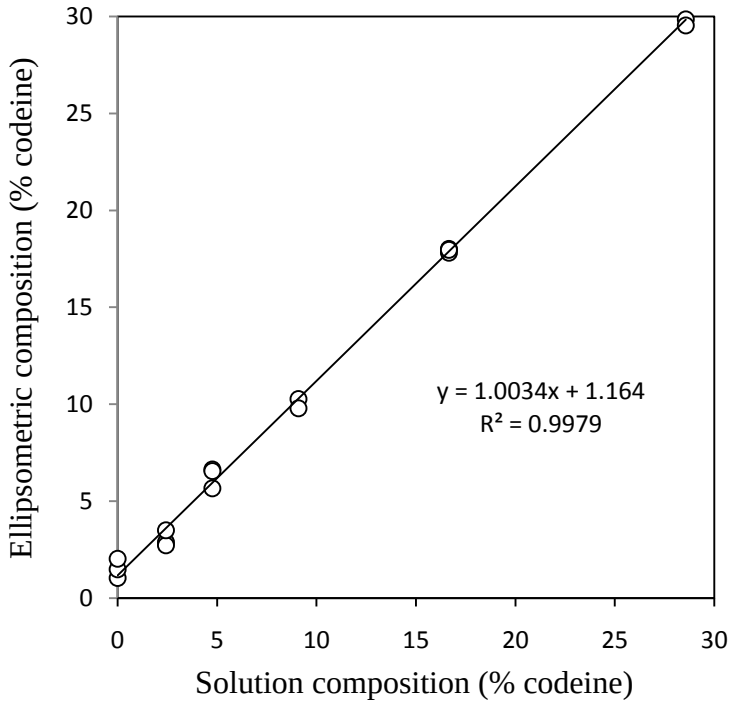

Figure 3.4 Ellipsometrically derived composition from the EMA model (as described in 3.2.2) against the known solution composition of PLA and PLA/codeine ranging from 0% to 28.6% (w/w) codeine.

With the compositional uniformity across a range of samples confirmed using the EMA model to determine the ellipsometric composition, it was judged that the films were appropriate for quantitative and qualitative assessment using XPS and ToF-SIMS depth profiling for a range of drug loadings.

3.3.3 XPS

The elements contained in PLA that are detected by XPS are carbon and oxygen, whereas codeine has one nitrogen atom per molecule within its structure. The chemical structures for PLA and codeine are shown in Figure 3.5a & b respectively. Thus, using the nitrogen concentration, the concentration of codeine through the XPS analysis depth of the film may be calculated.

a)

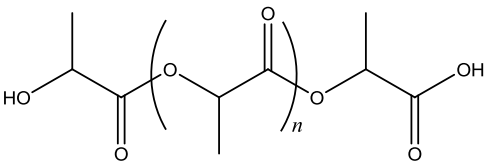

b)

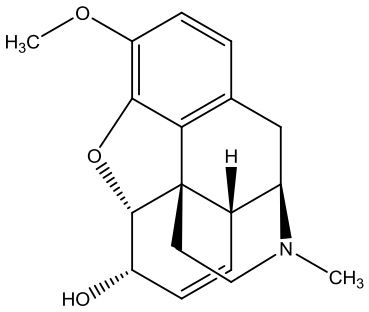

Element (PLA)	C	O
Elemental Ratio (Expected %)	3 (60%)	2 (40%)

Element (Codeine)	C	O	N
Elemental Ratio (Expected %)	18 (82%)	3 (13.5%)	1 (4.5%)

Figure 3.5 Molecular structure of a) PLA and b) codeine with elemental ratios tabulated.

The elemental composition of the surface of the six films with different codeine loading was determined with XPS, analysis of the nitrogen composition is presented against drug loading in Figure 3.6. The nitrogen concentration was found to be linearly proportional to the codeine loading ($R^2 = 0.9966$), calculated from the concentration of the solution used to spin cast the film. This is in agreement with the ellipsometric data and model shown in Figure 3.4. It was apparent that the measured nitrogen concentration was significantly lower than the nitrogen concentration calculated assuming uniform distribution of the codeine for all loadings (dashed line) indicating depletion of codeine at the surface (Figure 3.6). The surface depletion inferred from the measured nitrogen concentration was proportional to the codeine loading (Figure 3.6) suggesting that as the drug

loading increased, a constant proportion of codeine segregated away from the surface to the bulk of the film. An alternative explanation of this observation is an overlayer of constant thickness of PLA is formed on all samples that attenuates the bulk codeine signal by a constant factor for all drug loadings.

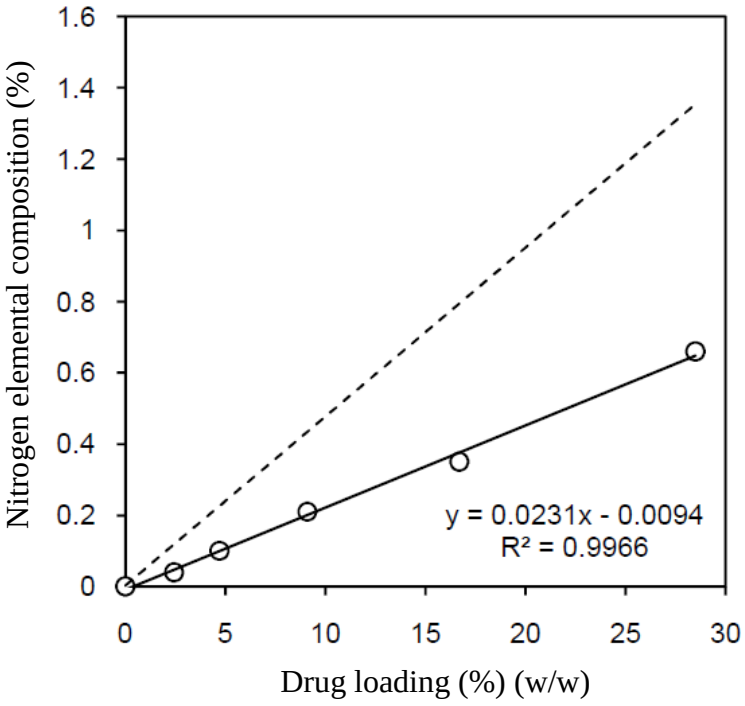

Figure 3.6 Observed XPS surface nitrogen elemental composition (%, ○) against drug loading (%, w/w). Solution concentration based on uniform distribution of the bulk loading (- - -) is also plotted. An average loss of 56.3% ± 5.9 from the calculated to the observed nitrogen concentration is observed at the surface.

To ascertain the depth scale, a uniform rate of sputtering through the sample film by the coronene source was assumed. This is an approach supported by other polyatomic sputtering investigations of PLA[10]. The time taken to reach the half maximum of the silicon substrate concentration was used with the depth of the sample film determined by ellipsometry to convert sputtering time to film thickness. The average sputter rate was 7.57 nm per 20 s sputter cycle with a standard deviation of 0.59. The XPS derived elemental composition determined after each coronene etching cycle is presented as a function of depth in Figure 3.7 for the sample with 28.6% (w/w codeine:PLA).

Again, surface depletion of codeine is suggested by the lower nitrogen concentration observed for the first point taken before coronene etching. Following further etching, the nitrogen concentration was observed to gradually increase and remain roughly constant within the bulk followed by a steep decline upon reaching the interface with the silicon wafer. The increase in the nitrogen signal observed with coronene etching is consistent with segregation of the codeine away from the surface to the bulk of the sample. The reduction in oxygen concentration seen in the same region (between 0 and 20 nm) is an indication of a zone of surface PLA enrichment. This trend, relative to each calculated solution drug loading, was observed for all other films analysed. This is in agreement with the systematically lower nitrogen concentrations seen in the analysis of films across the range of codeine loadings presented in Figure 3.7. From the nitrogen profile in Figure 3.7a, the zone of codeine depletion/ polymer enrichment at the surface may be up to 20 nm thick since a steady state is attained after this depth. The nitrogen concentration observed for three drug loadings is displayed in Figure 3.7b all show a zone of depletion, with enrichment found in the bulk. The zone of codeine depletion appears to be greater with the highest drug loading. Assuming a uniform sputter rate with the coronene source this observation suggests higher drug loadings have a thicker zone of PLA surface enrichment. ToF-SIMS depth profiling would be used to compare and contrast with the XPS depth profiles.

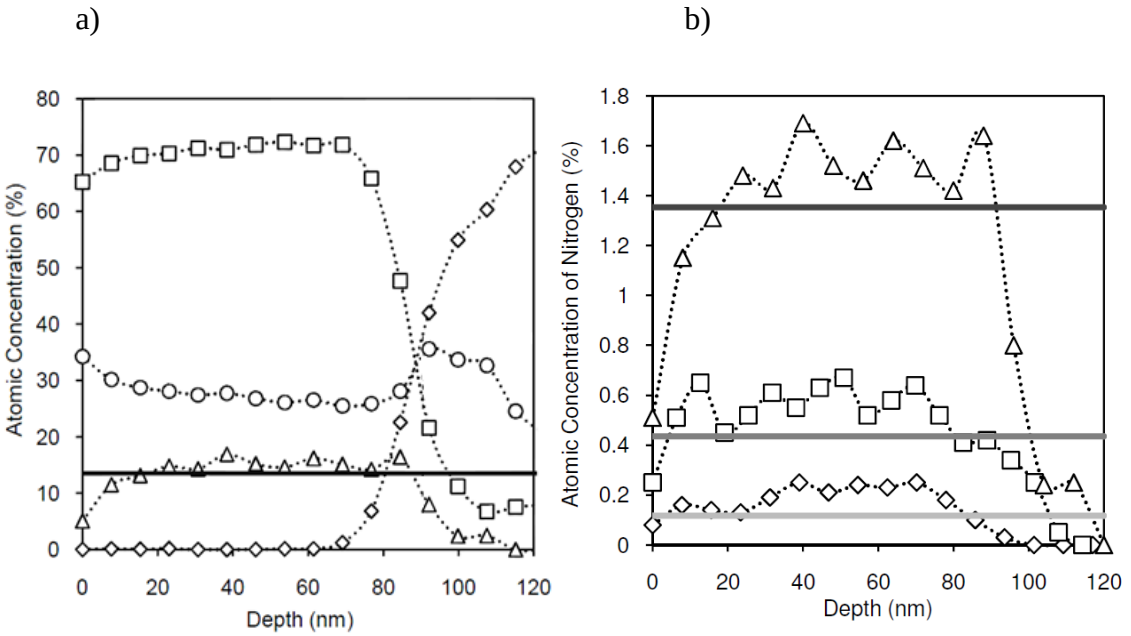

Figure 3.7 a) XPS depth profile from coronene etched 28.6% drug loaded film showing C1s (□), O1s (○), N1s × 10 (△), Si2p (◇) and the calculated nitrogen concentration assuming uniform drug distribution × 10 (▬) through film thickness. b) Nitrogen atomic concentration for 2.4% (◇, ▬), 9.1% (□, ▬) and 28.6% (△, ▬) with corresponding nominal concentration through thickness plotted.

The observed enrichment of PLA at the surface suggests partial segregation of PLA to the surface and codeine to the bulk. This would act to reduce the surface free energy of the film and this could be the driving force. In contrast, depth profiling ToF-SIMS of PLA and PLGA, blended with pluronic surfactant and sirolimus respectively, indicated that both the surfactant and drug segregated to the surface[27-29]. Alternatively, rapid evaporation of highly volatile chloroform in the spin coating procedure may encourage surface segregation of PLA if the polymer chains do not have time to reach equilibrium and as such may be "frozen" at the air/film interface as noted previously for a polymer blend containing polystyrene and poly(methyl-methacrylate)[30]. The data does not provide conclusive evidence on which, if either, mechanism is behind the surface enrichment of PLA/depletion of codeine.

The relatively gradual rise in silicon intensity with depth seen in Figure 3.7 implies that there is a broad interface (~ 40 nm range of silicon intensity) between the polymer and the substrate wafer, which through AFM analysis of the silicon wafer is known not to be the case for the silicon (2.46 nm roughness). The ~ 40 nm range over which the interface occurs is broader than values typically found with ToF-SIMS depth profiling[31]. Various factors are known to affect the vertical depth resolution as a function of sputtering depth including the depth of analysis, intermixing in the crater and roughening, with the last contribution dominant when performing ToF-SIMS depth profiling, but the first may be significant in XPS analysis[32]. When considering the 2.5 mm^2 area sputtered this is far greater than those used for conventional ToF-SIMS depth profiling as such, beam induced surface roughness is likely to be a considerable factor in limiting the depth resolution attainable.

To investigate the functional composition of the sputtered surfaces, component peaks for the C1s spectrum were chosen based upon the shape of the core level envelope. Binding energy shifts from the C-C environment from the pure PLA and pure codeine samples were consistent with literature values[33]. They were applied with fixed relative intensities based on the pure compounds to the core levels shown in Figure 3.8a. The C1s core levels acquired from the surface were fitted well by the set of component curves determined from both pure PLA and codeine when fixed at the same relative intensities for each individual component. Upon sputtering it was observed that the actual concentration of the C-O environment is reduced to a level lower than can be accommodated by the core level model using the individual pure components illustrated in Figure 3.8b. This small decrease in the relative intensity of the C-O environment of the sputtered surface is assigned to chain scission of PLA at the ester linkage forming a carboxyl group under coronene sputtering, the same trend after sputtering is seen in the pure PLA control sample shown in Figure 3.8c and d. No damage to the codeine could be discerned from the C1s fits of the drug loaded PLA, although the relatively low intensity of the codeine components in the C1s core level would make any such changes difficult to detect. The functional composition of the PLA-codeine surface was determined from curve fitting of the C1s region and is plotted versus depth in Figure 3.8e.

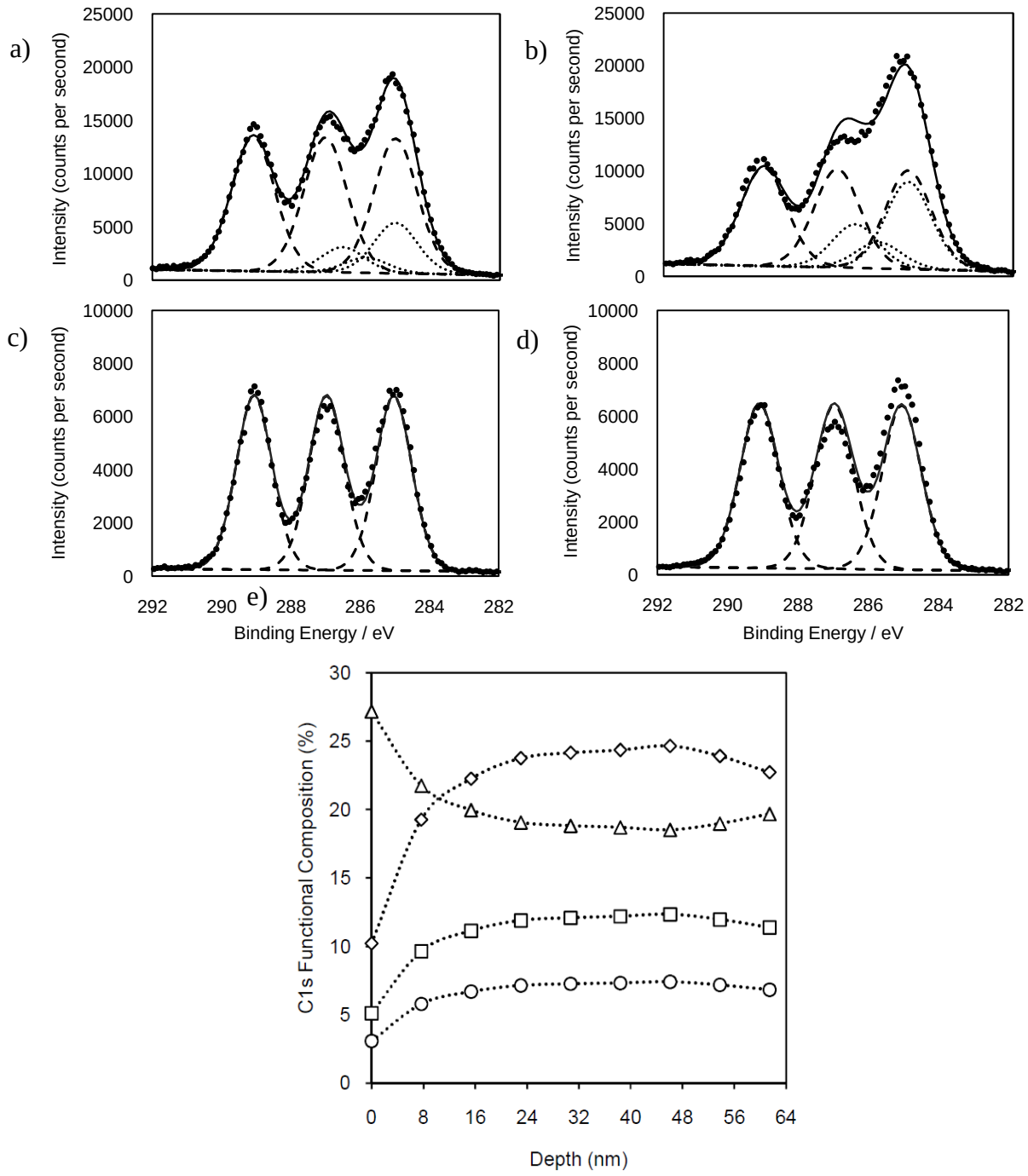

Figure 3.8 a) XPS spectra of C 1s region of the 28.6% drug loading at depth = 0 nm b) and depth = 8 nm charge corrected to the C-C at 285 eV. The model fit (▬), the XPS trace (●), PLA components (▬ ▬) and codeine components (▪▪▪▪) are plotted. c) Pure PLA control sample at depth = 0 nm d) and depth = 32 nm e) Functional composition of the C 1s region of the 28.6% drug loading plotted. Codeine component C-C (◇), C-O (□) and C-N (○). All PLA components are denoted by (△). Within the bulk of the film the actual codeine loading ranges between 30 and 35% (w/w codeine:PLA).

Two components were noted for the N1s region of the XPS spectra across all samples. These correspond to nitrogen within the codeine molecule and a protonated nitrogen environment. It is proposed that a hydrogen atom from carboxylic acid PLA end groups protonate a constant proportion of the codeine nitrogen atoms to produce this signal. This proposal is supported by the observation that the amount of protonated amine remains constant with increased codeine loading. The components of the N1s region for the 28.6% codeine loading remain at a constant ratio throughout the film thickness of 1:1.8 ($R_3\underline{N}H^+$:$\underline{N}R$) (not shown). The use of monatomic argon for traditional XPS depth profiling has been shown to degrade organic films significantly[16, 34]; however the effect of damage on the functional composition using coronene is shown to be minimal and allows for accurate quantitative analysis of organic material through film thickness.

The formulation process assumes that drug loading is constant throughout the film and since the kinetics of drug release will be dependent on the concentration profile within the film this information is extremely important in rationalising and predicting the performance of drug loaded polymer devices. It is shown that it is possible to use XPS to determine a significant drug depletion or enrichment from the surface. This could be used to understand anomalous drug release behaviour such as the observed burst effect found where the rate of drug elution from the polymer film is far higher than expected within the first hours following implantation[27-29].

Previously PLA films have been shown to be sputtered at a constant rate when using C_{60}^+ primary ions, indicating that depth profiling of film thicknesses greater than those used in this study is possible using cluster ion sources[10]. The technique is capable of using an aperture to allow acquisition from large areas simultaneously, these experiments used an aperture measuring 110 × 110 μm, however areas of up to 300 × 700 μm can be analysed. These results lay the foundations for future work monitoring the distribution of drug in simulated conditions thereby enabling elution profile interpretation using XPS depth profiling.

3.3.4 ToF-SIMS

All ToF-SIMS analyses in this chapter show ions from the positive spectra. It is these ions extracted which provide the most valuable information for the PLA in the thin films described previously[35]. The molecular ion of codeine used in this model can also be found in the positive spectrum. It is vital when selecting secondary ions to represent components within a film that they should be; intense, demonstrate negligible transient effects, be unique to a single component and have intensity proportional to the amount of material present. The identification of suitable secondary ions is best performed from pure materials without contaminant overlayers such as PDMS. The reference spectrum generated for both PLA and codeine are shown in Figure 3.9a and b respectively.

a)

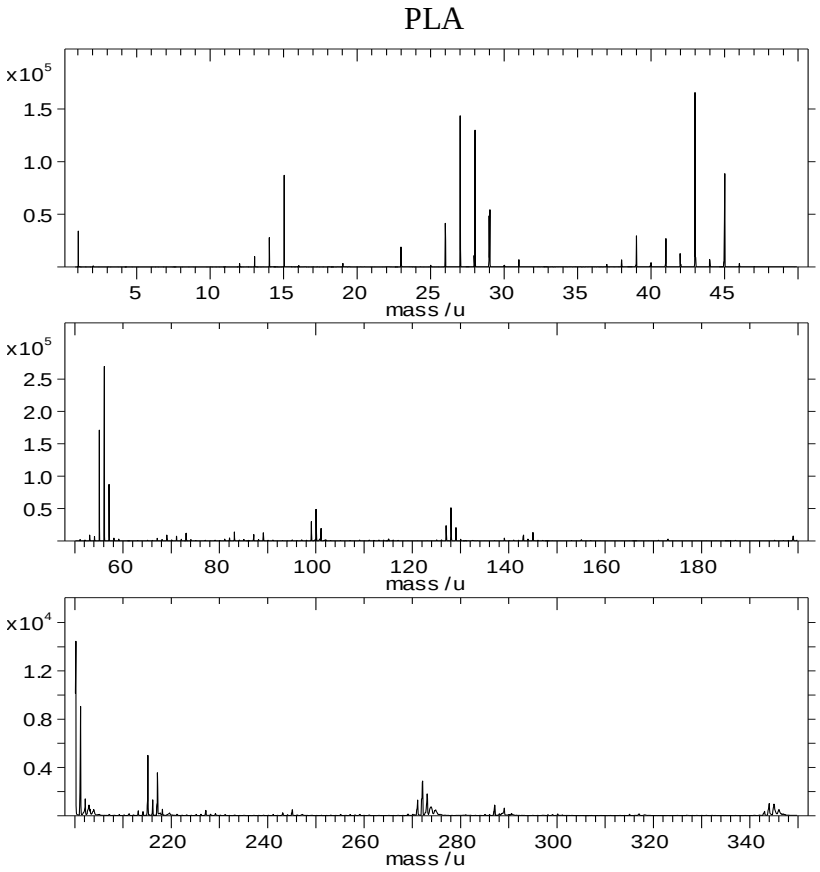

b)

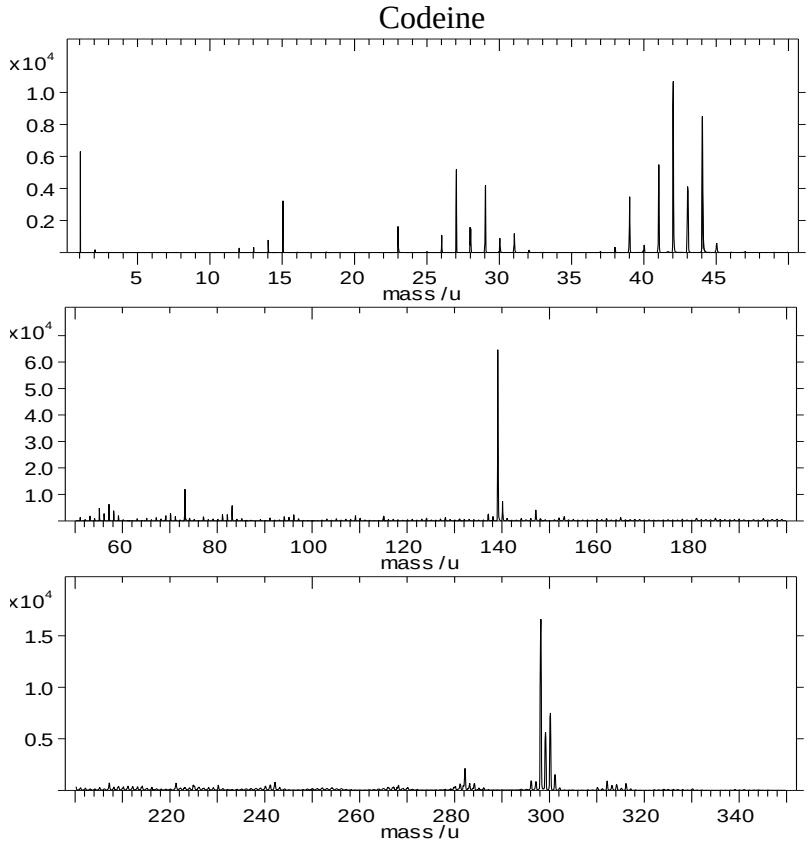

Figure 3.9 Positive ion ToF-SIMS spectra of a) PLA and b) codeine reference samples.

The reference spectra for PLA shows intense peaks which agree with those described elsewhere[35-37]. The fragmentation of pure PLA has been extensively analysed previously[36, 38]. Peaks at *m/z* 55, 56 (a radical cation which has been investigated previously that displays remarkable stability and intensity in ToF-SIMS of PLA[39]) and 57 are assigned to $C_3H_3O^+$, $C_3H_4O^{\bullet+}$, and $C_3H_5O^+$ respectively. They are all highly intense for PLA in the positive spectrum.

The structure of PLA shown in Figure 3.5a like many polymers forms $[M\pm H]_n^+$, $[M+O\pm H]_n^+$ and $[M-O\pm H]_n^+$ cations where M represents the repeating unit ($C_3H_4O_2$ for PLA) and n represents the number of repeating units. The three intense ions described here relate to a breakage at the ester linkage in the PLA chain forming intense $[M-O\pm H]_n^+$ cations and a radical. This ester linkage breaking under sputtering is also observed under coronene sputtering quantitatively by XPS depth profiling that further supports this method of chain scission of PLA chains to be taking place.

However not all these ions are best suited for a comparison with quantitative depth profiling as some are more susceptible to the surface transient effects as shown in Figure 3.10a and reported in the literature[5, 31, 40]. The transient change depends upon a balance between damage accumulation and precursor formation. High mass secondary ions more commonly show significant transient declines in intensity as displayed in Figure 3.10. High mass PLA fragments were therefore avoided for characterisation and *m/z* 55 was used to indicate PLA in all ToF-SIMS data shown in this chapter.

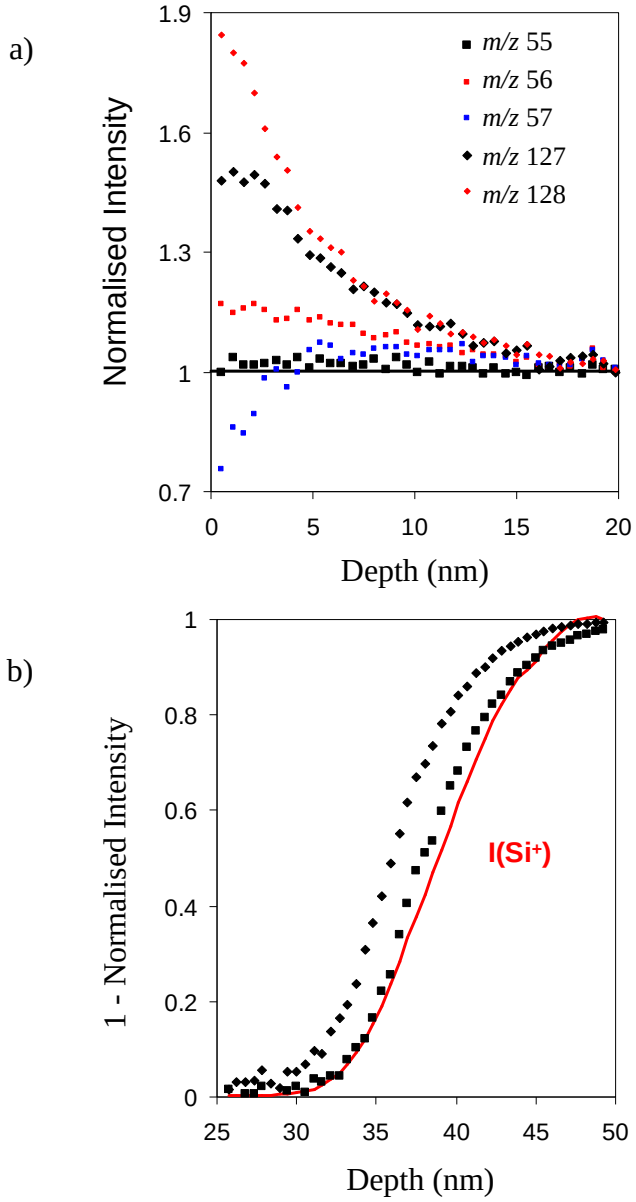

Figure 3.10 a) Comparison of PLA indicating secondary ion fragments intensity variation in the transient region of depth profiles. b) Normalised ion intensities for *m/z* 127 (◆) and *m/z* 55 (■) subtracted from unity and compared to the normalised Si^+ intensity for a 10 mg/ml solution of 28.6% (w/w) codeine/PLA.

It is assumed within a steady state regime, characteristic secondary ion intensity is proportional to the fractional area of material within the analysis region[41]. If this is the case then, at the interface between PLA and silicon, there should be an anti-correlation between ions characteristic of the two materials. To test this, the secondary ion intensities of two PLA ions ($C_3H_3O^+$, *m/z* 55; $C_6H_7O_3^+$, *m/z* 127) normalised to their maximum intensity, have been plotted against the secondary ion intensity of Si^+, normalised to its maximum intensity in Figure 3.10b. Whilst neither of the poly(lactide) secondary ion intensities provide a perfect fit to the silicon intensity, it is clear that the lower mass ion gives a better description in this region. In fact, the anti-correlation shown by the $C_3H_3O^+$ and Si^+ secondary ions in this plot is rather flattering, since there has been no attempt to account for the decline in Si^+ secondary ion intensity upon exposure to C_{60}^+ ion sputtering[10] after the removal of the SiO_2 layer described in Chapter 2. The important point is that lower mass secondary ions are preferable in this region of the depth profile as well as during the initial transient region because their intensities more closely correlate with the fractional area of their parent material.

The reference sample for codeine shown in Figure 3.9b highlights peaks which overlap with PLA however peaks at *m/z* 44, 139 (radical cation) and 300 (molecular ion) correspond respectively to $C_2H_6N^+$, an unidentified cation and $C_{18}H_{22}NO_3^+$ which are intense secondary ions unique to the codeine sourced. The spectra obtained is in agreement with electron ionisation mass spectrometry (EI-MS) data of the drug[42] other than the intensity of the ion at *m/z* 139. The radical cation was ~20 fold lower in intensity than the molecular ion when depth profiling but expressed a comparable depth profile to the two identified fragments. In Figure 3.9 it appears this radical cation at *m/z* 139 is most intense when codeine is in its solid powder form but when dissolved in chloroform and cast with PLA is degraded in intensity suggesting it may be a highly unstable radical and is affected by the solvent, PLA or spin casting process. As such the high intensity low mass ion $C_2H_6N^+$, *m/z* 44 was used to signify the presence of codeine.

The analysis of the surface of the polymer films with ToF-SIMS cannot be easily used to determine composition in a quantitative manner due to matrix affects described in Chapter 2. While ToF-SIMS is a qualitative technique, recently it has

been shown that ion intensities can be used to understand the film composition through a mathematical model[40].

The intensity of codeine secondary ions across a range of drug loadings are displayed in Figure 3.11 taken from surface spectra normalised to the total ion counts.

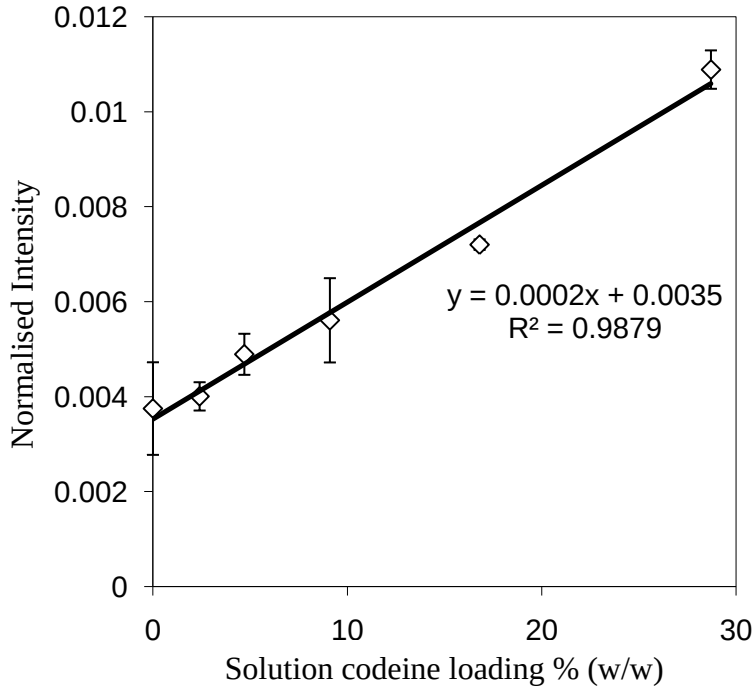

Figure 3.11 ToF-SIMS ion intensity normalised to total ion counts for the *m/z* 300 codeine molecular ion for drug loadings ranging from 0% to 28.6% (w/w).

A strong linear relationship is observed with respect to the codeine ion intensity with an increase in codeine loading, supporting the observation made of the ellipsometric and XPS data obtained. There is a remarkable congruency between the data from XPS shown in Figure 3.6 and the codeine intensities derived at the surface with ToF-SIMS. This suggests matrix affects described in Chapter 2 are less problematic in ToF-SIMS analysis of the binary drug polymer systems produced in this case.

A typical ToF-SIMS depth profile is shown in Figure 3.12 for the 28.6% (w/w) codeine drug loading that is representative of the repeatable results obtained. The

depth scale is derived using the same technique described for the XPS depth profiling based on the method described by Shard *et al*. 2007 [10, 43].

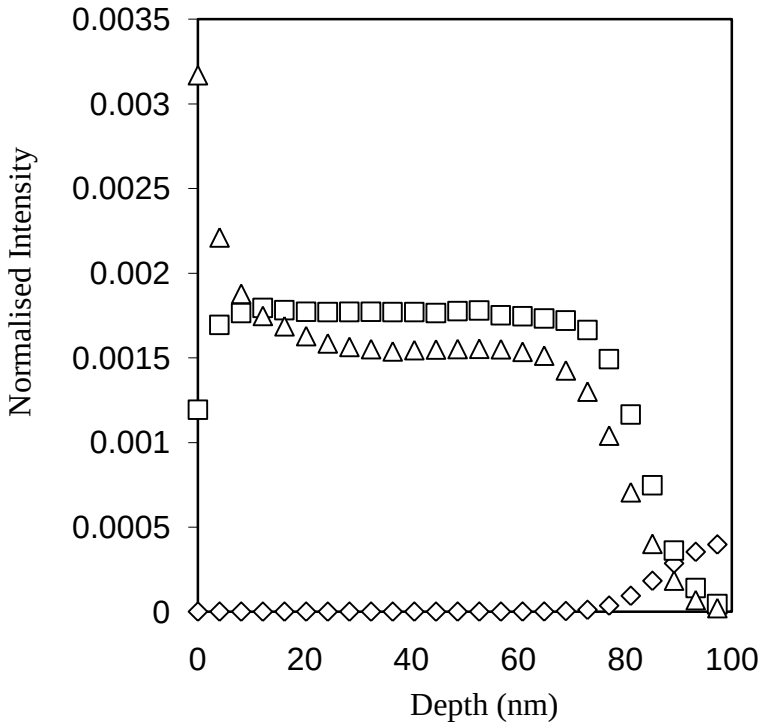

Figure 3.12 Representative ToF-SIMS depth profile of a 28.6% codeine loaded binary blend film measuring 91 nm in thickness, Si *m/z* 28 (◇), PLA *m/z* 55 (△) and codeine *m/z* 44 (□).

The depth profiles observed suggests slight codeine depletion at the surface which is less striking than that observed with XPS and polymer enrichment in the near surface transient region of the depth profiles. The width of the surface transient region is greater in XPS than with ToF-SIMS. This is likely to be due to the lower depth resolution of XPS. Alternatively the coronene source used in this work was a new and commercially unavailable source the uniformity of sputtering was largely unknown. As such this broadened near surface region may be due to a ion beam induced roughening/ topography generation or non-uniformity of sputtering[31]. The likelihood of topography caused by the casting process is low considering nominally produced films were analysed with AFM and ToF-SIMS indicating any such broadening may be sputtering related.

The increase in codeine signal in the transient phase indicates a possible enrichment of codeine at the immediate sub-surface. A mechanism through which

this may occur is due to an enhanced surface segregation of codeine caused by localised heating in the vicinity of a C_{60} impact[40]. This would depend upon material properties such as relative mobilities, surface energies and phase properties[40]. However the data from XPS (Figure 3.7) do not conclusively support this hypothesis as the analysis depth is between 5 and 10 nm with XPS. Hence the first or second data point would be expected to be greatest in intensity, assuming sub-surface enrichment and uniform sputtering. However the ToF-SIMS depth profiles of codeine shown with a linear scale in Figure 3.13 indicated surface depletion and only in the case of the highest drug loading does there appear to be any evidence of sub-surface enrichment. Should the intensity of the codeine representing ion decrease significantly after the surface transient ~15 nm has been sputtered through this would support a significant sub-surface segregation of drug. As this is not observed, ToF-SIMS supports the results of the XPS depth profiling. The depth profiling of the polymer blends by ToF-SIMS was highly reproducible with variation in codeine intensity being related to the solution drug composition as shown in Figure 3.13 using a linear scale.

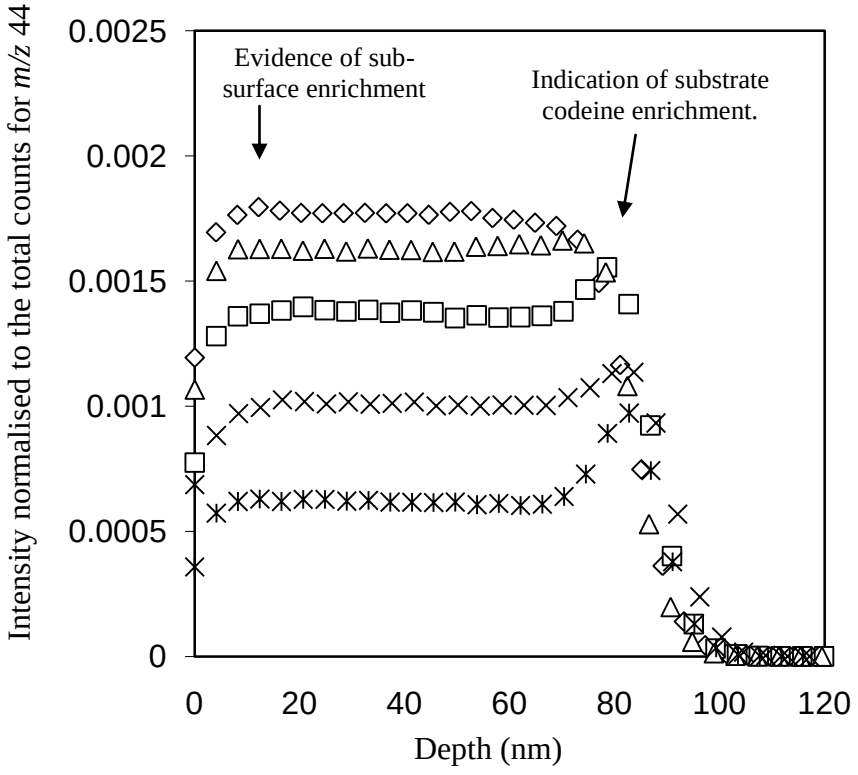

Figure 3.13 Depth profiles of 2.4% (✳), 4.7% (×) 9.1% (□), 16.8% (△) and 28.6% (◇) (w/w) codeine.

A broad depletion of codeine from the surface is shown by XPS however the zone of codeine depletion in ToF-SIMS is sharper than that illustrated by XPS measuring ~12 nm in ToF-SIMS. This may be due to the use of interlaced mode for ToF-SIMS depth profiling where both the sputtering and analysis beams are working simultaneously, whereas due to the relatively long acquisition time required for XPS, cycles of sputtering and analysis had to be adhered to. The interlaced mode used for ToF-SIMS data acquisition is responsible for the smoother data obtained with the ToF-SIMS than the XPS, as data is acquired at narrower intervals.

On reaching the interface with the silicon wafer there is an additional zone of codeine enrichment which is more pronounced for the lower drug loadings (Figure 3.13). At the silicon wafer the energy at which primary ions impact the harder inorganic surface increases causing more energetic primary ion impacts[44]. Such impacts may increase the secondary ion yield in addition to valid codeine enrichment at the silicon interface. The data obtained suggests this observation is a real enrichment of codeine at the interface, which may be amplified by the secondary ion yield enhancement. Higher drug loadings express the interfacial enrichment to a lesser degree, this observation may be due to greater saturation of the PLA bulk with drug reducing the observed interface saturation. It is noted the PLA signal (not shown) does not increase at the silicon interface further supporting a real enrichment at the silicon interface in lower drug loadings. XPS may not be sensitive enough for this model where one nitrogen atom in the codeine structure is required for its characterisation to fully represent any silicon interface enrichment for the lower drug loadings.

When comparing the data it is also important to understand how the sampling depth of XPS is between 5 and 10 nm whereas the ToF-SIMS is specific to the top 1-2 nm of the sample. This would allow for greater depth resolution at the expense of quantification. The analysis shows the complementary nature of ToF-SIMS and XPS for depth profiling, bringing depth resolution and quantification respectively. This allows for a thorough understanding of the drug distribution through thickness which otherwise would not be possible.

3.4 Conclusions

Through the combined use of ellipsometry, AFM, XPS and ToF-SIMS of spun cast films, both before and after sputtering with coronene and C_{60} ions. In this work the ability to both quantitatively and qualitatively conclude that surface depletion of drug occurs in the polymer films is demonstrated. For the first time the ability to directly quantify the variation of drug levels within such films with depth profiling XPS analysis has been described. XPS and ToF-SIMS have been compared with respect to their depth profiling capabilities. While ToF-SIMS appears to provide improvements to depth resolution the problems encountered with using sputtering sources on organics are evident in both techniques. XPS however is able to more easily show the specific nature of the damage done by sputtering than with ToF-SIMS. The ability to interrogate the drug distribution levels within such polymer films will provide a greater insight into the influence of fabrication processes on film formation and also on the subsequent drug release kinetics from polymeric drug eluting biomaterials.

This analysis however has been shown to be limited by the use of a model system measuring ~100 nm thick. A study on a flat film version of a real world drug eluting stent containing the anti-cancer drug sirolimus indicated strong surface enrichment of drug[45]. As polymeric stent films used in industry are often ~ 7 μm in thickness and it has been shown that thin spun cast films can have chemical characteristics that are uncharacteristic of thicker films[46]. However the benefit of such a thin model system is shown by interfacial effects such as the initial transient region in depth profiling and the indication of a non-linear intensity response occurring at the organic film-inorganic substrate interface are observed and provide a greater understanding of the dynamics of sputtering organic material before the depth has become too great and a loss of secondary ion intensity is observed[41].

3.5 References

1. Braun, R.M., J. Cheng, E.E. Parsonage, J. Moeller, and N. Winograd, *Analytical Chemistry*, 2006. **78**(24): p. 8347-8353.
2. Kang, E., H. Wang, I.K. Kwon, Y.H. Song, K. Kamath, K.M. Miller, J. Barry, J.X. Cheng, and K. Park, *Journal of Biomedical Materials Research Part A*, 2008. **87A**(4): p. 913-920.
3. Belu, A.M., M.C. Davies, J.M. Newton, and N. Patel, *Analytical Chemistry*, 2000. **72**(22): p. 5625-5638.
4. van der Weerd, J. and S.G. Kazarian, *Journal of Controlled Release*, 2004. **98**(2): p. 295-305.
5. Mahoney, C.M., S.V. Roberson, and G. Gillen, *Analytical Chemistry*, 2004. **76**(11): p. 3199-3207.
6. Belu, A.M., D.J. Graham, and D.G. Castner, *Biomaterials*, 2003. **24**(21): p. 3635-3653.
7. Huang, N.P., R. Michel, J. Voros, M. Textor, R. Hofer, A. Rossi, D.L. Elbert, J.A. Hubbell, and N.D. Spencer, *Langmuir*, 2001. **17**(2): p. 489-498.
8. Cheng, J., J. Kozole, R. Hengstebeck, and N. Winograd, *Journal of the American Society for Mass Spectrometry*, 2007. **18**(3): p. 406-412.
9. Mollers, R., N. Tuccitto, V. Torrisi, E. Niehuis, and A. Licciardello, *Applied Surface Science*, 2006. **252**(19): p. 6509-6512.
10. Shard, A.G., P.J. Brewer, F.M. Green, and I.S. Gilmore, *Surface and Interface Analysis*, 2007. **39**(4): p. 294-298.
11. Mahoney, C.M. and A.J. Fahey, *Analytical Chemistry*, 2008. **80**(3): p. 624-632.
12. Mahoney, C.M., A.J. Fahey, G. Gillen, C. Xu, and J.D. Batteas, *Applied Surface Science*, 2006. **252**(19): p. 6502-6505.
13. Sjovall, P., D. Rading, S. Ray, L. Yang, and A.G. Shard, *Journal of Physical Chemistry B*. **114**(2): p. 769-774.
14. Biddulph, G.X., A.M. Piwowar, J.S. Fletcher, N.P. Lockyer, and J.C. Vickerman, *Analytical Chemistry*, 2007. **79**(19): p. 7259-7266.
15. Chen, Y.Y., B.Y. Yu, W.B. Wang, M.F. Hsu, W.C. Lin, Y.C. Lin, J.H. Jou, and J.J. Shyue, *Analytical Chemistry*, 2008. **80**(2): p. 501-505.
16. Tanaka, K., N. Sanada, M. Hikita, T. Nakamura, T. Kajiyama, and A. Takahara, *Applied Surface Science*, 2008. **254**(17): p. 5435-5438.
17. Miyayama, T., N. Sanada, S.-i. Iida, J.S. Hammond, and M. Suzuki, *Applied Surface Science*, 2008. **255**(4): p. 951-953.
18. Sanada, N., A. Yamamoto, R. Oiwa, and Y. Ohashi, *Surface and Interface Analysis*, 2004. **36**(3): p. 280-282.
19. Bachman, B.J. and M.J. Vasile, *Journal of Vacuum Science & Technology A: Vacuum, Surfaces, and Films*, 1989. **7**(4): p. 2709-2716.
20. Hwang, J., F. Amy, and A. Kahn, *Organic Electronics*, 2006. **7**(5): p. 387-396.
21. Ogaki, R., *Surface Analysis of Biodegradable Polymer-Drug Binary Blends*. 2007, University of Nottingham.
22. DeLongchamp, D.M., R.J. Kline, D.A. Fischer, L.J. Richter, and M.F. Toney, *Advanced Materials*. **23**(3): p. 319-337.
23. Xie, H., J. Wei, and X. Zhang, *International Conference on Materials for Advanced Technologies (ICMAT 2005)*, 2006. **28**: p. 95-99.

24. Aspnes, D.E., *Thin Solid Films*, 1982. **89**(3): p. 249-262.
25. Gabriele, S., P. Damman, S. Sclavons, S. Desprez, S. Coppee, G. Reiter, M. Hamieh, S. Al Akhrass, T. Vilmin, and E. Raphael, *Journal of Polymer Science Part B-Polymer Physics*, 2006. **44**(20): p. 3022-3030.
26. Zhang, F.J., G. Baralia, A. Boborodea, C. Bailly, B. Nysten, and A.M. Jonas, *Langmuir*, 2005. **21**(16): p. 7427-7432.
27. Zolnik, B.S. and D.J. Burgess, *Journal of Controlled Release*, 2008. **127**(2): p. 137-145.
28. Narasimhan, B. and R. Langer, *Journal of Controlled Release*, 1997. **47**(1): p. 13-20.
29. Belu, A., C. Mahoney, and K. Wormuth, *Journal of Controlled Release*, 2008. **126**(2): p. 111-121.
30. Tanaka, K., A. Takahara, and T. Kajiyama, *Macromolecules*, 1996. **29**(9): p. 3232-3239.
31. Wagner, M.S., *Analytical Chemistry*, 2004. **77**(3): p. 911-922.
32. Shard, A.G., F.M. Green, P.J. Brewer, M.P. Seah, and I.S. Gilmore, *The Journal of Physical Chemistry B*, 2008. **112**(9): p. 2596-2605.
33. Beamson, G.B., D, *The XPS of Polymers Database in High Resolution*. 2000, SurfaceSpectra Ltd.
34. Hollander, A., M. Haupt, and C. Oehr, *Plasma Processes and Polymers*, 2007. **4**(9): p. 773-776.
35. Davies, M.C., R.D. Short, M.A. Khan, J.F. Watts, A. Brown, A.J. Eccles, P. Humphrey, J.C. Vickerman, and M. Vert, *Surface and Interface Analysis*, 1989. **14**(3): p. 115-120.
36. Shard, A.G., C. Volland, M.C. Davies, and T. Kissel, *Macromolecules*, 1996. **29**(2): p. 748-754.
37. Davies, M.C., A. Brown, J.M. Newton, and S.R. Chapman, *Surface and Interface Analysis*, 1988. **11**(12): p. 591-595.
38. Ogaki, R., F.M. Green, I.S. Gilmore, A.G. Shard, S. Luk, M.R. Alexander, and M.C. Davies, *Surface and Interface Analysis*, 2007. **39**(11): p. 852-859.
39. Short, R.D. and M.C. Davies, *International Journal of Mass Spectrometry and Ion Processes*, 1989. **89**(2-3): p. 149-155.
40. Shard, A.G., A. Rafati, R. Ogaki, J.L.S. Lee, S. Hutton, G. Mishra, M.C. Davies, and M.R. Alexander, *Journal of Physical Chemistry B*, 2009. **113**(34): p. 11574-11582.
41. Shard, A.G., F.M. Green, P.J. Brewer, M.P. Seah, and I.S. Gilmore, *Journal of Physical Chemistry B*, 2008. **112**(9): p. 2596-2605.
42. Watson, D.G., *Pharmaceutical Analysis*. 1999, London: Elsevier Science Limited. 337.
43. Rafati, A., M.C. Davies, A.G. Shard, S. Hutton, G. Mishra, and M.R. Alexander, *Journal of Controlled Release*, 2009. **138**(1): p. 40-44.
44. Green, F.M., I.S. Gilmore, and M.P. Seah, *Rapid Communications in Mass Spectrometry*, 2008. **22**(24): p. 4178-4182.
45. Fisher, G.L., A.M. Belu, C.M. Mahoney, K. Wormuth, and N. Sanada, *Analytical Chemistry*, 2009. **81**(24): p. 9930-9940.
46. Shard, A.G., M.C. Davies, S.J.B. Tendler, D.E. Jackson, P.N. Lan, E. Schacht, and M.D. Purbrick, *Polymer*, 1995. **36**(4): p. 775-779.